

Vibrational energies for the \tilde{X}^1A_1 , \tilde{A}^1B_1 , and \tilde{B}^1A_1 states of $\text{SiH}_2/\text{SiD}_2$ and related transition probabilities based on global potential energy surfaces

Ikuo Tokue and Katsuyoshi Yamasaki

Department of Chemistry, Faculty of Science, Niigata University, Ikarashi, Niigata 950-2181, Japan

Shinkoh Nanbu

Computer Center, Institute for Molecular Science, Myodaiji, Okazaki 444-8585, Japan

(Received 15 December 2004; accepted 28 January 2005; published online 8 April 2005)

Transition probabilities were evaluated for the \tilde{X}^1A_1 - \tilde{A}^1B_1 and \tilde{A}^1B_1 - \tilde{B}^1A_1 systems of SiH_2 and SiD_2 to analyze the $\tilde{X} \rightarrow \tilde{A} \rightarrow \tilde{B}$ photoexcitation. The Franck–Condon factors (FCFs) and Einstein's B coefficients were computed by quantum vibrational calculations using the three-dimensional potential energy surfaces (PESs) of the SiH_2 ($\tilde{X}^1A_1, \tilde{A}^1B_1, \tilde{B}^1A_1$) electronic states and the electronic transition moments for the \tilde{X} - \tilde{A} , \tilde{X} - \tilde{B} , and \tilde{A} - \tilde{B} system. The global PESs were determined by the multireference configuration interaction calculations with the Davidson correction and the interpolant moving least-squares method combined with the Shepard interpolation. The obtained FCFs for the \tilde{X} - \tilde{A} and \tilde{A} - \tilde{B} systems exhibit that the bending mode is strongly enhanced in the excitation since the equilibrium bond angle greatly varies with the three states; the barrier to linearity is evaluated to be $21\,900\text{ cm}^{-1}$ for the \tilde{X} state, 6400 cm^{-1} for the \tilde{A} state, and 230 – 240 cm^{-1} for the \tilde{B} state. The theoretical lifetimes for the pure bending levels of the \tilde{A} and \tilde{B} states were calculated from the fluorescence decay rates for the \tilde{A} - \tilde{X} , \tilde{B} - \tilde{A} , and \tilde{B} - \tilde{X} emissions.

© 2005 American Institute of Physics. [DOI: 10.1063/1.1876112]

I. INTRODUCTION

The silylene radical is one of the simplest molecules containing silicon. Interest in silylene became greater recently because of the important role of silicon hydride molecules in fabricating amorphous silicon. Very many data are accumulated on the \tilde{X}^1A_1 and \tilde{A}^1B_1 states by both experimental and theoretical methods, whereas there has been only a little amount of information about the \tilde{B} state.^{1,2} Very recently, the \tilde{A}^1B_1 - \tilde{B}^1A_1 absorption spectrum of SiH_2 and SiD_2 has been analyzed in the 9500 – $12\,000\text{ cm}^{-1}$ using IR double resonance spectra of $\text{SiH}_2/\text{SiD}_2$ prepared by photodissociation of phenyl silane.³ To analyze these spectra we need several spectroscopic constants that depend on the vibrational state for both electronic states.

Many theoretical studies treated SiH_2 , which represents the strong Renner–Teller (RT) interaction.⁴ We would like to review here only some of the important studies related to the present work. Rice and Handy,¹ and Gordon⁵ reported the equilibrium structures and potential energy surfaces (PES) for several electronic states of SiH_2 obtained by multiconfiguration self-consistent field (MCSCF) calculations. Balasubramanian and McLean,⁶ and Yamaguchi *et al.*² calculated the equilibrium structures and a singlet-triplet splitting in SiH_2 by complete active space self-consistent field-second order configuration interaction (CASSCF-SOCI) method. Allen and Schaefer III⁷ obtained the harmonic vibrational frequencies based on the configuration interaction singles

and doubles (CISD) energies. Koseki and Gordon⁸ calculated the vibrational structure of the \tilde{X} - \tilde{A} absorption spectrum based on two-dimensional MCSCF/6-31G** PESs of the lowest three states. Gabriel *et al.*⁹ obtained the rotational-vibrational spectrum of the \tilde{X}^1A_1 and \tilde{a}^3B_1 states based on the three-dimensional PES and electric dipole moment functions.

Unfortunately, the published data regarding vibrational energies have been found to be inadequate especially for the \tilde{B} state. We therefore obtained these data by a three-dimensional calculation in the present study. Three-dimensional PESs of SiH_2 ($\tilde{X}, \tilde{A}, \tilde{B}$) ions were obtained by an *ab initio* molecular orbital (MO) configuration interaction (CI) method, and three-dimensional transition moments were obtained for the \tilde{X} - \tilde{A} , \tilde{X} - \tilde{B} , and \tilde{A} - \tilde{B} systems. Next, we carried out quantum vibrational calculations on these PESs to obtain the vibrational eigenvalues and eigenfunctions and acquired the Franck–Condon factors (FCFs) and the transition probabilities for the \tilde{X} - \tilde{A} , \tilde{X} - \tilde{B} , and \tilde{A} - \tilde{B} excitations. We also obtained those for SiD_2 . The present paper outlines first the *ab initio* MO CI calculations used in our determination of the PESs, as well as quantum vibrational calculations. Subsequently, we describe the PESs for the \tilde{X}^1A_1 , \tilde{A}^1B_1 , and \tilde{B}^1A_1 states and also vibrational states for each electronic state. Finally, the obtained FCFs and Einstein's B coefficients are summarized and the fluorescence lifetimes evaluated from

both Einstein's B coefficients and the transition frequencies are compared with other data.

II. THEORETICAL CALCULATIONS

A. *Ab initio* MO CI calculations

Determination of the global PES is quite important for calculations of the higher vibrational states, as it is necessary to take into account the anharmonicity of the PES, especially for the electronic excited states. Details in calculation of PESs and vibrational energies were reported previously.¹⁰ The basis set used in the present work was the aug-cc-pVQZ (diffusion-function-augmented, correlation consistent, polarized valence, quadruple zeta) of Woon and Dunning.¹¹ The MOs were determined by CASSCF calculations. After determining the MOs, multireference configuration interaction (MRCI) calculations were carried out.

SiH_2 is a 16-electron system, and the ground state for the valence is approximated by a two-configuration wave function²

$$C_1[\text{core}](4a_1)^2(2b_2)^2(5a_1)^2 - C_2[\text{core}] \\ \times (4a_1)^2(2b_2)^2(2b_1)^2 \tilde{X}^1 A_1,$$

where $|C_1| > |C_2|$.

The first excited singlet state is an open shell and may be written as

$$[\text{core}](4a_1)^2(2b_2)^2(5a_1)^1(2b_1)^1 \tilde{A}^1 B_1.$$

The second and final excited singlet state studied in this work is again a closed shell and may be written as

$$C_2[\text{core}](4a_1)^2(2b_2)^2(5a_1)^2 + C_1[\text{core}] \\ \times (4a_1)^2(2b_2)^2(2b_1)^2 \tilde{B}^1 A_1.$$

The two lowest \tilde{X} and \tilde{A} states are derived from ${}^2\Pi_u$ from the RT interaction, and correlate with the $\text{H}_2(X^1\Sigma^+) + \text{Si}({}^1D_g)$ system in the dissociation limit. The \tilde{B} state correlates with the same $\text{H}_2(X^1\Sigma^+) + \text{Si}({}^1D_g)$ system. Moreover, the \tilde{X} and \tilde{A} states correlate with the $\text{SiH}(X^2\Pi) + \text{H}({}^2S)$ channel, which is 1.7 eV higher than the $\text{H}_2(X^1\Sigma^+) + \text{Si}({}^1D_g)$ channel, whereas the \tilde{B} state correlates with the $\text{SiH}(A^2\Delta) + \text{H}({}^2S)$ channel. To obtain the MOs necessary to describe these electronic states, the state-averaged CASSCF calculations were carried out with inclusion of a full valence as the active space orbitals. The active space of the MRCI calculations is the same as that of CASSCF, and the configuration state functions were generated by single and double excitations with respect to the reference configurations used in the CASSCF calculation, except for the frozen-core orbitals, $1s$, $2s$, and $2p$ (Si). Moreover, the Davidson correction for the MRCI calculation was employed to include the correlation energy due to higher excitations.¹²⁻¹⁴ The total number of configurations for the final internally contracted MRCI calculations was typically around 523 000 for the A' symmetry and 262 000 for the A'' symmetry.^{15,16} In the present work, the potential energies for the electronic ground state, $1^1A'$, and the next two electronic excited states, $1^1A''$ and $2^1A'$,

were finally obtained in the C_s symmetry. The transition dipole moments between these states were evaluated from the CI wave functions. All calculations were carried out with the MOLPRO program package.¹⁷ The computer was an SGI Origin 2800 owned by the Research Center for Computational Science at Okazaki.

Jacobi coordinates were employed to describe the relative positions of the three nuclei in the body fixed plane; r is the distance between the two H atoms, R is the distance between the Si atom and the center of mass of two H atoms, and θ is the angle between the vectors R and r . Potential energies and transition dipole moments for SiH_2 were calculated at 6500 geometries and were interpolated by the interpolant moving least-squares method combined with the Shepard method¹⁸⁻²⁰ to carry out a quantum vibrational calculation on the PESs. The parameters to determine the weight functions [see Eq. (6) of Ref. 18] were chosen to be $a=0.03$ and $p=4$.

B. Quantum vibrational calculations

Since some of the highly vibrational excited states could be characterized with the unlocalized wave function that does not look like the zero-point vibrational wave function, we performed a quantum vibrational calculation based on the discrete variable representations.²¹⁻²⁴ The Hamiltonian matrix and associated wave functions are represented with evenly spaced grids in R and r , and associated Legendre polynomials to describe $\cos \theta$. The grid parameters were suitable for the radial part: ($N_R=109, R_{\min}=0.0a_0, R_{\max}=8.0a_0$) and ($N_r=79, r_{\min}=2.0a_0, r_{\max}=8.0a_0$), where N is

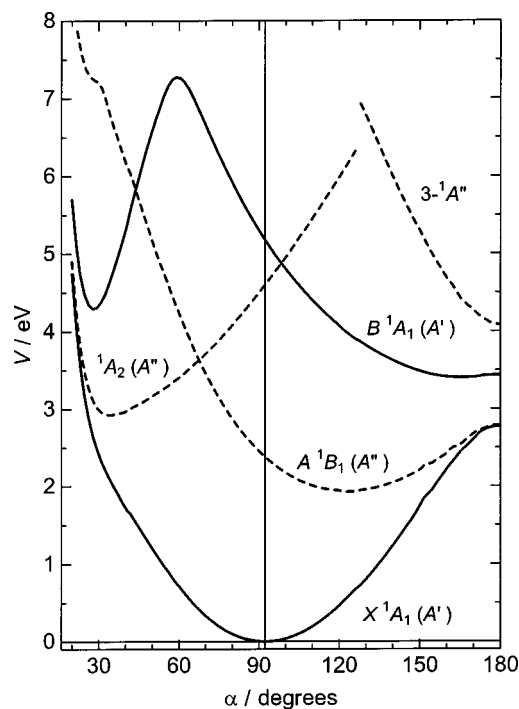


FIG. 1. Potential energies for the \tilde{X}^1A_1 , \tilde{A}^1A_2 and \tilde{B}^1A_1 states in eV as a function of α ; r_{SiH} is fixed at the equilibrium length of 1.5187 Å for the ground state, and the solid and dashed curves represent the A' and A'' states, respectively. The vertical line near 92° represents the equilibrium angle for the ground state.

TABLE I. Equilibrium geometries of SiH₂ and electronic energies; the Si–H bond length is in angstrom, the H–Si–H angle α in degrees, and the energy difference from the \tilde{X}^1A_1 state (ΔE_e) in eV.

State	r_{SiH} (Å)	α (deg)	ΔE_e (eV)	Method
\tilde{X}^1A_1	1.5187	92.27		MRCI, Present
	1.5148	92.42		CISD/B2 ^b
	1.5168	92.04		CEPA ^c
	1.5124	92.74		CISD ^d
	1.5141	92.08		IR absorption ^e
	1.5140	91.98		IR absorption ^f
\tilde{A}^1B_1	1.4904	122.70	1.9218	MRCI, Present
	1.4833	122.53	2.0372	CISD/B2 ^b
	1.4814	122.87	1.9936	CISD ^d
	1.4853	122.44		IR absorption ^f
			1.9256 ^a	LIF ^g
\tilde{B}^1A_1	1.4690	164.83	3.3480	MRCI, Present
	1.4577	162.27	3.5556	CISD ^d
\tilde{a}^3B_1	1.4825	117.77	0.9121	MRCI, Present
	1.4768	118.30	0.8478	CISD/B2 ^b
	1.4793	118.43	0.8626	CEPA ^c
	1.4760	118.24	0.8856	CISD ^d
3A_1	1.6486	180.0	0.91±0.03 ^a	PIMS ^h
			3.1818	MRCI, Present

^a ΔE_0 value.^bReference 7.^cReference 9.^dReference 2.^eReference 27.^fReference 28.^gReference 29.^hReference 30.

the number of grid points and a_0 is the Bohr radius. The number of Legendre functions was 60 for the angular part. The method adopted for the diagonalization of the Hamiltonian matrix is the implicitly restricted Lanczos method.²⁵ In the present work, assuming the total angular momentum $J=0$ and 1, the lowest 200 vibrational states were obtained for the three electronic states of SiH₂ and SiD₂. The FCFs were then evaluated as the square of the overlap integrals between the initial and final states for the \tilde{X} - \tilde{A} , \tilde{X} - \tilde{B} , and \tilde{A} - \tilde{B} systems, and the electronic transition probabilities for photoabsorption²⁶ were also evaluated as the square of the transition moments that depend on both the initial and final vibrational states.

III. RESULTS AND DISCUSSION

A. Potential energy surfaces

The equilibrium geometry of each state was calculated via polynomial fit for the potential energy data. Table I summarizes the geometries thus determined compared with the published data. Theoretical geometries obtained in this study are in good agreement with both the experimental^{27,28} and recent theoretical data,^{2,7,9} and our excitation energies to the \tilde{A}^1B_1 and \tilde{a}^3B_1 states agree with the observed ΔE_0 values^{29,30} better than the other theoretical values.^{2,7,9} Figure 1 shows the potential energy curves for the five lowest states in SiH₂, where r_{SiH} is fixed at the equilibrium length of 1.5187 Å for the \tilde{X} state. It is clearly seen that there is a

Renner–Teller pair of the \tilde{X}^1A_1 and \tilde{A}^1B_1 states at around the linear conformation. Potential energy surfaces of SiH₂ obtained by the present study are very similar to those obtained for SiH₂⁺ calculated by the SOCI method reported by Mort *et al.*³¹ despite of the different spin state. Although the \tilde{A}^1B_1 and 1A_2 states cross each other at around $\alpha=70^\circ$, these states avoid crossing due to the same symmetry A'' because the molecular symmetry comes to the lowest symmetry C_s . Thus, the vibrational states of the \tilde{A}^1B_1 and 1A_2 states can be mixed due to the nonadiabatic transitions. Furthermore, the rovibrational mixing of the \tilde{X}^1A_1 and \tilde{A}^1B_1 states can occur due to the RT coupling, which is also a nonadiabatic process. However, in the present work, keeping the adiabaticity of the electronic states, we applied the Franck–Condon analysis to this system for understanding the photoexcitation mechanism.

Figure 2 shows the PESs of the \tilde{X} , \tilde{A} , and \tilde{B} states, where r is fixed at the equilibrium for each state. The energy zero of each electronic state is taken to be at the global energy minimum of the corresponding state; \tilde{X}^1A_1 , \tilde{A}^1B_1 , and \tilde{B}^1A_1 are $-290.183\,908$, $-290.113\,285$, and $-290.060\,870 E_h$, respectively. The equilibrium R distances for the excited states are shorter than that for the \tilde{X} state as shown in Fig. 2, indicating that the bending progression should be dominant in the excitation from the \tilde{X} state according to the Franck–Condon principle.

The values for the electric dipole moment of the \tilde{X} , \tilde{A} ,

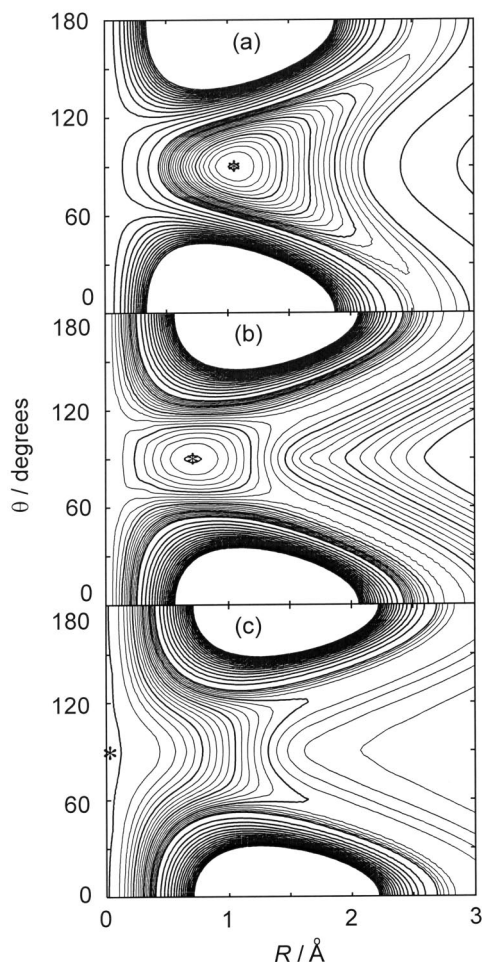


FIG. 2. Potential energy surfaces for the (a) \tilde{X} , (b) \tilde{A} , and (c) \tilde{B} states; r is fixed at the equilibrium distance for each state. The asterisk represents the potential minimum. Narrow and thick contours are shown in the interval of 0.2 and 1.0 eV, respectively.

and \tilde{B} states at the equilibrium geometry for the ground state are 0.0762, -0.1888 , and -0.3736 a.u., respectively. Figure 3 shows the dependence of the electronic dipole and transition dipole moments M on α with $r_{\text{SiH}}=1.5187$ Å, which is the equilibrium length for the \tilde{X} state; M_y^{XX} , M_y^{AA} , and M_y^{BB} are the electric dipole moments for the \tilde{X} , \tilde{A} , and \tilde{B} states, respectively, and M_z^{XA} and M_z^{AB} are the transition dipole moments for the \tilde{X} - \tilde{A} and \tilde{A} - \tilde{B} systems, respectively. The dependence of the electric dipole moments on α and their magnitude are mainly originated in the contribution of the $5a_1$ orbital. M_y^{BB} suddenly changes at $\alpha < 70^\circ$ because of the avoided crossing as shown in Fig. 1. M_z^{XA} and M_z^{AB} decrease at $\alpha \geq 80^\circ$ and become zero at $\alpha = 180^\circ$. Although M_z^{XA} and M_z^{AB} increase with decreases in r , the contribution from these areas to the pure bending transitions is expected to be small since the potential energies for all the states increase steeply with deviating r from the equilibrium distance.

B. Vibrational analysis

The \tilde{A} state exhibits a conical intersection around $r_{\text{SiH}}=1.5$ Å, $\alpha=68^\circ$, 3.6 eV above the \tilde{X} state minimum. Since there is considerable mixing between the diabatic state in a

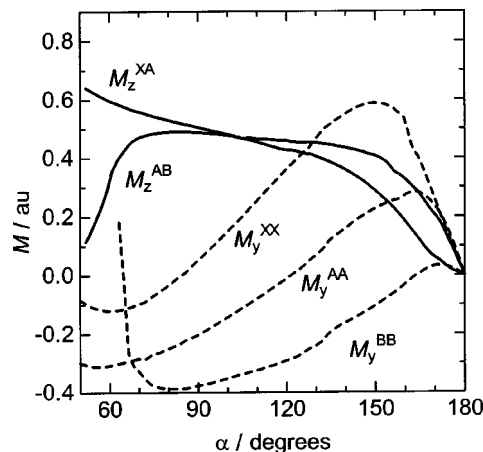


FIG. 3. Electric dipole (dashed curve) and transition dipole (solid curve) moments as a function of α , with $\theta=90^\circ$ and $r_{\text{SiH}}=1.5187$ Å; the M_y^{XX} , M_y^{AA} , and M_y^{BB} are the electric dipole moments for the \tilde{X} , \tilde{A} , and \tilde{B} states, respectively, and the M_z^{XA} and M_z^{AB} are the transition dipole moments for the \tilde{X} - \tilde{A} and \tilde{A} - \tilde{B} systems, respectively.

region around the intersection region, vibrational energies with $J=0$ and 1 were calculated up to $10\,000$ cm^{-1} from the potential minimum of the \tilde{A} state. Those energies for the \tilde{B} state were calculated up to 9000 cm^{-1} since the \tilde{B} state correlates to the dissociating $\text{Si}(^2\text{D})+\text{H}_2$ channel. For all the states of SiH_2 and SiD_2 , the vibrational quantum numbers (ν_1, ν_2, ν_3) have been assigned up to 80 levels. To certify the assignment, a least-square analysis was applied to the vibrational frequencies of the levels with $\nu_1 + \nu_3 \leq 4$ using the well-known formula for three normal vibrations including anharmonicity constants; the vibrational frequency in reference to the vibrational ground state is given by³²

$$G(\nu_1, \nu_2, \nu_3) = \sum_{i=1}^3 \omega_i^0 \nu_i + \sum_{i=1}^3 \sum_{k \geq i}^3 x_{ik}^0 \nu_i \nu_k. \quad (1)$$

For the \tilde{B} state, the degenerate formula was applied for the bending modes ν_2 . For all the states the vibrational levels with $\nu_1 + 0.5 \nu_2 + \nu_3 \leq 2$ were successfully analyzed, whereas the $\nu_1 + 0.5 \nu_2 + \nu_3 \geq 3$ levels were deviated definitely from this formula. Therefore, we added the third-order anharmonicity constants y_{222} to Eq. (1) and considered Fermi and Darling-Dennison-type resonances.^{32,33} The vibrational levels for the \tilde{X} , \tilde{A} , and \tilde{B} states of SiH_2 and SiD_2 up to 80 levels were successfully fitted by the analysis.

We should take Coriolis coupling into account for the rigorous analysis since the calculated vibrational energies of the states with $J=1$ include the Coriolis interaction. For $\text{SiH}_2(\tilde{X})$, Yamada *et al.*²⁷ derived that the interaction matrix element between ν_2 and ν_3 is 0.7 cm^{-1} and that between ν_1 and ν_3 is 9 cm^{-1} . Although we did not find any experimental data of the Coriolis coupling constants for the \tilde{A} and \tilde{B} states, the interaction may not be large especially between ν_2 and ν_3 . Therefore, we neglected the effect of Coriolis interaction in the vibrational analysis because our goal of this study is to describe the feature of the $\tilde{X} \rightarrow \tilde{A} \rightarrow \tilde{B}$ excitation as a whole.

TABLE II. Comparison of calculated and observed vibrational energies in cm⁻¹ for the nonrotating \tilde{X}^1A_1 state of SiH₂ and SiD₂; the symmetric stretching ν_1 , bending ν_2 , and antisymmetric stretching ν_3 modes.

(ν_1, ν_2, ν_3)	SiH ₂				SiD ₂		
	Present	Expt.	Obs.-Calc.	Theor. ^d	Present	Expt. ^e	Obs.-Calc.
(0,1,0)	987	998.6 ^a	12	997	719	719.8	1
(0,2,0)	1954	1987.7 ^b	34	1992	1423	1444.6	22
(0,3,0)	2911	2998.6 ^c	88	3023	2122		
(0,4,0)	3855	3997.5 ^c	143	4043	2814		
(0,5,0)	4786				3499		
(0,6,0)	5708				4177		
(0,7,0)	6625				4847		
(0,8,0)	7536				5513		
(0,9,0)	8441				6178		
(0,10,0)	9338				6840		
(0,0,1)	1987	1992.8 ^b	-6		1449	1439.1	-10
(1,0,0)	1999	1995.9 ^b	-3	2015	1454	1426.9	-27
(1,1,0)	2972	2952.7 ^c	-19	2973	2165		
(1,2,0)	3927	3923.3 ^c	-4	3960	2865		
(1,3,0)	4876				3549		
(1,4,0)	5816				4228		
(1,5,0)	6712				4908		
(1,6,0)	7631				5582		
(1,7,0)	8547				6246		
(1,8,0)	9458				6908		
(0,0,2)	3908	3952.0 ^b	44		2855		
(1,0,1)	3918				2866		
(2,0,0)	3986	3976.8 ^c	-7	4008	2900		

^aReference 27.^bReference 34.^cReference 35.^dReference 9.^eReference 36.

To examine the accuracy of the PESs, especially concerning the bending mode, the vibrational frequencies obtained in this study are compared with other data. Table II summarizes the vibrational energies for the ground state with $J=0$ of SiH₂ and SiD₂ compared with data obtained by experiments^{27,34-36} and the other theoretical study.⁹ The present result reproduces the condition $\nu_1 > 2\nu_2$ established by Hirota and Ishikawa.³⁴ Although the difference between our results and the observed result for the bending states seems to increase with the vibrational energy, the difference is roughly estimated to be within 10% up to the (0,10,0) level. These differences may not cause serious problem because we are interested in the FCF from the lower vibrational levels of the \tilde{X} state.

Table III summarizes the vibronic energies for the \tilde{A}^1B_1 state with $J=0$ comparing with observed data; we did not find any theoretical value except harmonic frequencies.⁷ The term value T_e calculated for the \tilde{A} state seems to be slightly larger than the observed T_0 value.²⁹ For the T_e value, we should mention that we have adopted 15 400 cm⁻¹, which was subtracted by 100 cm⁻¹ from the calculated values to compare the vibronic energies with the observed data.^{29,37,38} The present vibronic energies are in fairly good agreement with the observed values despite of the deviation to the higher side. The deviation does not seem to be accumulated for higher levels. When $J=0$ ($K=0$), the RT coupling is rig-

orously neglected, whereas the RT interaction should be included in the states with $J > 0$ in the rigorous treatment of the vibrational energy and the transition probability. Duxbury *et al.*⁴ successfully reproduced the observed vibronic energies for the \tilde{A} state including the RT coupling and the spin-orbit coupling with the \tilde{a}^3B_1 state. In preliminary calculation with the same method reported by Goldfield *et al.*,³⁹ the RT effect on the vibronic energies was estimated for the states with $J = 1$ of SiH₂. Table IV lists the results including the RT coupling compared with those neglecting the RT effect and the observed data.^{4,40,41} The RT coupling is found to be not large for the states with $\nu_2 \leq 2$, while the agreement with the observed vibrational states with $\nu_2 \geq 3$ is improved by including the RT interaction. This feature may originate in their geometry. The \tilde{A} state is characterized with the bend structure ($\alpha = 123^\circ$) as seen in Fig. 1. Although the RT effect is small for low bending states, the effect cannot be neglected with increasing the quantum number for the bending mode. The difference of the vibrational energy spaces for the lower states might be due to spin-orbit coupling, which should be mixed with the RT effect.

Although such a complex problem is one of the challenging systems which should be solved, our interest is a bit different from such a viewpoint; our purpose is to analyze the spectra related with the highly vibrational states and not to concentrate on the lower states. Of course, it should be

TABLE III. Comparison of calculated and experimental vibronic energies in cm^{-1} for the nonrotating \tilde{A}^1B_1 state of SiH_2 and SiD_2 .

(ν_1, ν_2, ν_3)	SiH_2			SiD_2		
	Present	Expt.	Obs.-Calc.	Present	Expt. ^a	Obs.-Calc.
(0,0,0)	15 454	15 546.0 ^a	92	15 425	15 550	125
(0,1,0)	16 390	16 405.7 ^a	16	16 124	16 168	44
(0,2,0)	17 307	17 247.8 ^a	-60	16 794	16 778	-16
(0,3,0)	18 202	18 095.5 ^a	-107	17 458	17 390	-68
(0,4,0)	19 070	18 935.8 ^a	-134	18 112	18 001	-111
(0,5,0)	19 901	19 776.0 ^a	-125	18 751	18 608	-142
(0,6,0)	20 678	20 618.8 ^a	-59	19 375	19 206	-169
(0,7,0)	21 384	21 468.0 ^a	84	19 980	19 808	-172
(0,8,0)	22 071	22 328.0 ^b	257	20 562	20 406	-156
(0,9,0)	22 834			21 099	21 003	-96
(0,10,0)	23 647			21 582	21 604	22
(0,11,0)	24 510			22 097		
(1,0,0)	17 487			16 901		
(0,0,1)	17 634			17 045		
(1,1,0)	18 411			17 593		
(1,2,0)	19 315	19 203.23 ^c	-112	18 260		
(1,3,0)	20 193	20 036.37 ^c	-157	18 919		
(1,4,0)	21 041	20 867.83 ^c	-173	19 565		
(1,5,0)	21 846	21 699.46 ^c	-147	20 194		
(1,6,0)	22 609			20 806		
(1,7,0)	23 325			21 394		
(2,0,0)	19 444			18 337		
(1,0,1)	19 538			18 446		
(0,0,2)	19 721			18 623		

^aReference 37.^bReference 38.^cReference 29.

needed to calculate the vibrational energies until much higher states both to make sure such an explanation and to calculate the transition probabilities more accurately on this convenient approximation for the RT effect. Unfortunately, the (0, 4, 0) level for the \tilde{A} state corresponds to the 515th state in the calculation and then the calculation including much higher states may exceed our available computational resource. Therefore, we neglected the RT effect in the calculation for the $J=1$ state since the difference between the vibronic energy neglected the RT effect and the observed does not seem to increase above the (0, 4, 0) state.

Tables V and VI summarize the vibronic energies for the levels with $J=0$ and 1, respectively, of the \tilde{B}^1A_1 states compared with observed data.³ Although there is not enough of the observed vibrational levels to compare the energy with the present data, the accuracy of the vibronic energies for the \tilde{B} state seems to be sufficient up to the (0,15,0) state in this calculation.

The barrier to linearity, which is the difference between the electronic energy for the equilibrium geometry and that for the optimized under linear constraint, is evaluated to be

TABLE IV. Calculated and observed rovibronic energies T_0 of the states with $J=1$ and $K=0$ for the $\text{SiH}_2(A)$ state.

(ν_1, ν_2, ν_3)	No RT ^a		RT ^b		Obs. ^c
	T_0	Obs.-Calc.	T_0	Obs.-Calc.	T_0
(0,0,0)	15 570		15 542		
(0,1,0)	16 506	-94	16 500	-88	16 412
(0,2,0)	17 424	-167	17 411	-154	17 257
(0,3,0)	18 321	-214	18 198	-91	18 107
(0,4,0)	19 193	-249	18 931	13	18 944
(0,5,0)	20 030	-245			19 785
(0,6,0)	20 825	-195			20 630

^aCalculation neglecting the RT effect.^bCalculation including the RT effect.^c $J_{KaKc}=1_{10}$ state; Refs. 4, 40, and 41.

TABLE V. Comparison of calculated vibronic energies in cm⁻¹ for the Σ levels with $J=0$ of the \tilde{B}^1A_1 state of SiH₂ and SiD₂ with experiment; $\nu_2=2 \nu_2^{\text{bent}}+K$.

(ν_1, ν_2, ν_3)	SiH ₂		SiD ₂	
	Present	Present	Expt. ^a	Obs.-Calc.
(0,0,0)	27 055	27 015	27 214	199
(0,2,0)	28 114	27 780	27 865	85
(0,4,0)	30 204	28 561	28 631	70
(0,6,0)	30 330	30 361		
(0,8,0)	31 488	30 179		
(0,10,0)	32 678	31 017		
(0,12,0)	33 890	31 872		
(0,14,0)	35 120	32 743		
(0,16,0)		33 625		
(1,0,0)	30 095	28 500		
(0,0,1)	30 220	28 603		
(1,2,0)	30 169	30 273		
(1,4,0)	31 259	30 057		
(1,6,0)	32 373	30 855		
(1,8,0)	33 515	31 668		
(1,10,0)	34 684	32 498		
(1,12,0)	35 873	33 343		
(2,0,0)	30 979	30 910		
(1,0,1)	31 097	30 014		
(0,0,2)	31 393	30 233		

^aReference 3.

21 900±170 cm⁻¹ for the \tilde{X} state, 6400±170 cm⁻¹ for the \tilde{A} state, and 230–240 cm⁻¹ for the \tilde{B} states. The barrier for the \tilde{B} state is about twice as that of 125 cm⁻¹ obtained from the spectroscopic analysis of SiD₂.³ This difference suggests that the double minimum for the \tilde{B} state is overestimated in this calculation. The theoretical term value for the (0,0,0) level of SiD₂ is remarkably lower than the observed compared with those for the excited bending levels. This deviation is evidently caused by the overestimation of the barrier to linearity.

C. Franck–Condon factors and transition probabilities for the \tilde{X} – \tilde{A} system

To evaluate the vibrational distribution of the \tilde{A}^1B_1 state in the photoexcitation of the ground state of SiH₂ and SiD₂, the FCFs were calculated for the band from the m state with $(\nu''_1, \nu''_2, \nu''_3)$ to the n state with (ν'_1, ν'_2, ν'_3) of the $\tilde{X} \rightarrow \tilde{A}$ excitation. Moreover, the Einstein's B coefficients for the same transition were calculated based on the three-dimensional

TABLE VI. Same as Table V but for the Π levels with $J=1$.

(ν_1, ν_2, ν_3)	SiH ₂			SiD ₂		
	Present	Expt. ^a	Obs.-Calc.	Present	Expt. ^a	Obs.-Calc.
(0,1,0)	27 585	27 650	65	27 397	27 455	58
(0,3,0)	28 657	28 745	88	28 168	28 219	51
(0,5,0)	30 763	*30 896	133	28 957	30 033	76
(0,7,0)	30 904			30 764		
(0,9,0)	32 078			30 591		
(0,11,0)	33 279			31 436		
(0,13,0)	34 499			32 307		
(0,15,0)	35 733			33 172		
(0,17,0)				34 058		
(1,1,0)	30 636	30 785	149	28 887		
(1,3,0)	30 715			30 664		
(1,5,0)	31 815			30 453		
(1,7,0)	33 042			31 256		
(1,9,0)	34 093			32 076		
(1,11,0)	35 274			33 012		
(1,13,0)				33 762		

^aReference 3; the number with the asterisk represents the mixed state.

transition dipole moment. In this study, Einstein's B coefficients for the $m \rightarrow n$ band in $\text{m}^3 \text{J}^{-1} \text{s}^{-2}$ units is given by

$$B_{nm} = 1.216\,67 \times 10^{20} |M_{nm}|^2, \quad (2)$$

where the transition moment M_{nm} is in atomic units.

Since the $\tilde{X}\text{-}\tilde{A}$ excitation is of a type C with $\Delta K = \pm 1$, the FCFs and Einstein's B coefficients are calculated for the $J = 0 \rightarrow 1$ ($K = 0 \rightarrow 1$) band from the $(0, \nu_2'' = 0-9, 0)$ levels for SiH_2 . The results are listed in Table A-I in the Appendix.⁴² In the same manner Table A-II in the Appendix lists those from the $(0, \nu_2'' = 0-10, 0)$ for SiD_2 . In the $\tilde{X}\text{-}\tilde{A}$ transition the change in r_{SiH} in equilibrium is only 0.028 \AA , while that in α is 30° . Therefore, the main band is the ν_2' progression. The bands to the $(1, \nu_2' = 0-8, 0)$ levels are next important especially in the excitation from the higher bending levels. The FCFs to the $(\nu_1', \nu_2', \nu_3' = \text{odd})$ states are zero since their wave functions have a node on the R - r plane at $\theta = 90^\circ$. The FCFs and Einstein's B coefficients of the $J = 1 \rightarrow 0$ ($K = 1 \rightarrow 0$) band coincide sufficiently well with the corresponding values for the $J = 0 \rightarrow 1$ ($K = 0 \rightarrow 1$) band. In this study the transition probabilities to the $(0, \nu_2', 0)$ levels from the $(0, 0, 0)$ level of the \tilde{X} state has a peak around $\nu_2' = 3-4$, which is slightly shifted to the higher side than those calculated by Koseki and Gordon.⁸ The transition dipole moment depends on the molecular geometry as described at Sec. III A, and then may depend on the vibrational bands. Nevertheless, we found that the dependence is not so serious and then estimated the transition probabilities averaged over the pure bending states $(0, \nu_2' = 0-10, 0)$. The averaged $|M|^2$ value is

$(0.23 \pm 0.02)e^2 a_0^2$, which agrees reasonably with the value of $0.26e^2 a_0^2$ deduced by Fukushima *et al.*,³⁷ and that of $0.30e^2 a_0^2$ calculated by Duxbury *et al.*,⁴ but is fairly smaller than that of $0.40e^2 a_0^2$ calculated by Koseki and Gordon.⁸

Einstein's A coefficients A_{nm} for the $n \rightarrow m$ band of the $\tilde{A} \rightarrow \tilde{X}$ emission, which are proportional to the cube power of the transition energy, were calculated from Einstein's B coefficients and the differences of the vibronic energies between the two states (see Tables A-I and A-II).⁴² The A_{nm} summed up with m of the \tilde{X} state corresponds the fluorescence decay rate of the n level of the \tilde{A} state; for the $J = 0$ state m was summed up to 200, and for the $J = 1$ state m up to 180. Figure 4 shows the theoretical lifetimes for SiH_2 and SiD_2 , which are the inverse of the fluorescence decay rate compared with the observed lifetimes^{37,38} and the calculated lifetimes.⁴ The agreement of the theoretical lifetimes with the experimental data is very satisfactory except those for $\nu_2 \leq 1$. The observed lifetime for SiH_2 decreases rapidly for $\nu_2 \geq 6$ compared with the theoretical value because of predissociation.^{37,38} Duxbury *et al.*⁴ studied the RT coupling between the \tilde{X} and \tilde{A} states and the spin-orbit coupling with the lowest triplet state, which cause strong rotational perturbations and anomalous fluorescence lifetimes. There is no RT effect for levels with $K = 0$. Our lifetimes for levels with $K = 1$ neglecting the RT interaction are rather shifted to lower side than those with $K = 0$ at higher ν_2 . This tendency is contrary to those obtained by Duxbury *et al.*⁴ It is concluded that the RT interaction considerably increases the fluorescence lifetimes of the $K = 1$ levels for SiH_2 with $\nu_2 \geq 6$. Nevertheless, the effect to those for SiD_2 with $\nu_2 \geq 8$ seems to be not so serious.

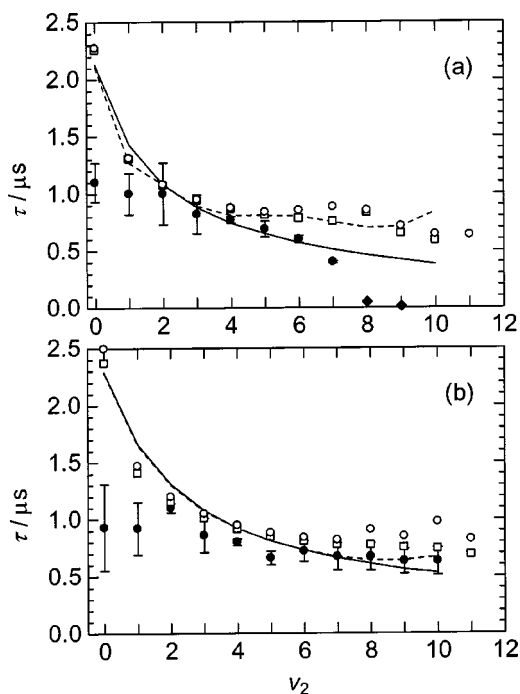


FIG. 4. Theoretical and experimental lifetimes for the pure bending states $(0, \nu_2, 0)$ of (a) $\text{SiH}_2(\tilde{A})$ and (b) $\text{SiD}_2(\tilde{A})$: the open circles and squares are theoretical values for the $J = 0$ and 1 ($K = 1$) levels, respectively, obtained in this study, the filled circles with error bar are the observed for the 0_{00} level taken from Fukushima *et al.* (Ref. 37), the filled diamonds are those taken from Francisco *et al.* (Ref. 38), and the solid and broken curves are calculated values for $K = 0$ and 1 , respectively, taken from Duxbury *et al.* (Ref. 4).

D. Franck-Condon factors and transition probabilities for the $\tilde{A}\text{-}\tilde{B}$ system

To evaluate the vibrational distribution of the $\tilde{B}^1 A_1$ state in the photoexcitation of the $\tilde{A}^1 B_1$ state of SiH_2 and SiD_2 , the FCFs and the Einstein's B coefficients were calculated for the $(\nu_1'', \nu_2'', \nu_3'') \rightarrow (\nu_1', \nu_2', \nu_3')$ band of the $\tilde{A} \rightarrow \tilde{B}$ transition. For SiH_2 , Table A-III in the Appendix⁴² lists the calculated FCFs and Einstein's B coefficients of the $J = 0 \rightarrow 1$ ($K = 0 \rightarrow 1$) band from the $(0, \nu_2'' = 0-10, 0)$ level, and Table A-IV lists those of the $J = 1 \rightarrow 0$ ($K = 1 \rightarrow 0$) band. Those for SiD_2 are summarized in Tables A-V and A-VI.⁴² In this transition the change in r_{SiH} in equilibrium is only 0.021 \AA , while that in α is 42° . Therefore, the main band is the ν_2' progression. The bands to the $(1, \nu_2' = 1-11, 0)$ and $(1, \nu_2' = 1-12, 0)$ levels are next important for the excitation with $\Delta K = 1$ and -1 , respectively. The transition probability was found to strongly depend on the vibrational state.

Einstein's A coefficients for pure bending levels of the \tilde{B} state were evaluated for the $\tilde{B}\text{-}\tilde{A}$ emission from Einstein's B coefficients and transition energies. The A_{nm} summed with m up to 200 for $J = 0$ and up to 180 for $J = 1$ of the \tilde{A} state. In the same manner, Einstein's A coefficients for pure bending levels were calculated for the $\tilde{B}\text{-}\tilde{X}$ system, which has a transition moment in the molecular plane. Figure 5 shows the

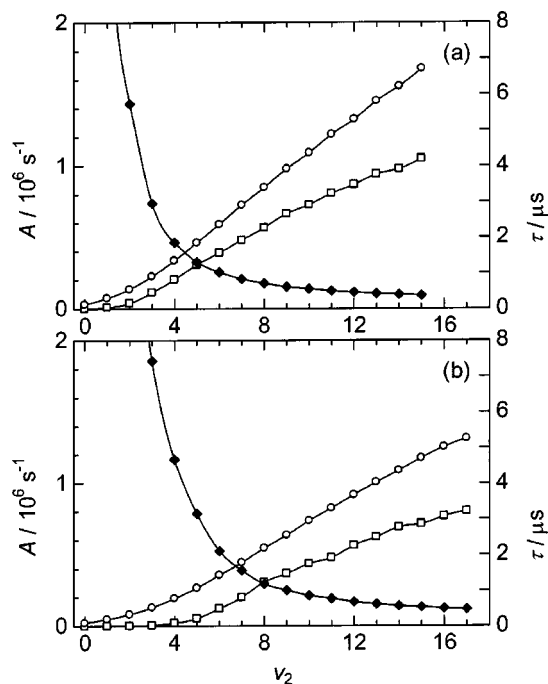


FIG. 5. Theoretical decay rates and radiative lifetimes for the pure bending states $(0, \nu_2, 0)$ of (a) SiH₂(\tilde{B}) and (b) SiD₂(\tilde{B}); open circles and squares are Einstein's A coefficients in 10^6 s^{-1} for the $\tilde{B}-\tilde{A}$ and $\tilde{B}-\tilde{X}$ emission, respectively, and filled diamonds are the radiative lifetimes in microseconds. The values of the states with $\nu_2 = \text{even}$ are for the $J=0$ level and those with $\nu_2 = \text{odd}$ are for the $J=1$ ($K=1$) level.

transition probabilities for the spontaneous emission of the $\tilde{B}-\tilde{A}$ and $\tilde{B}-\tilde{X}$ systems and the fluorescence lifetimes for the pure bending levels of the \tilde{B} state for SiH₂ and SiD₂. The fluorescence lifetime of the \tilde{B} state rapidly decreases with increases in ν_2 , and becomes shorter than those for the \tilde{A} state at higher bending levels probably because of the contribution from the $\tilde{B}-\tilde{X}$ emission. The \tilde{B} state correlates with the Si(¹D)+H₂(X) channel. Therefore, the lifetimes of the higher vibrational levels are expected to be shorter than the theoretical values because of predissociation. Muramoto *et al.*³ observed a line broadening of some rotational transitions in the $\tilde{A}-\tilde{B}$ absorption spectrum. To clarify the origin of this broadening we are now studying theoretically the dynamics in the SiH₂(\tilde{B}) → Si(¹D)+H₂(X) dissociation.

IV. CONCLUSION

The PESs of the \tilde{X} , \tilde{A} , and \tilde{B} states of the silylene radical were obtained from the CASSCF/MRCI method with the aug-cc-pVQZ basis sets in this study. The vibrational energies were calculated up to 200 levels for these electronic states of SiH₂ and SiD₂ and the vibrational states were assigned up to 80 levels. The accuracy of the vibrational energies calculated for the \tilde{X} state is estimated to be very good. The vibronic energies for the \tilde{A} and \tilde{B} states agree well with the observed data. A comparison of the calculated vibrational energy for the $(0,0,0)$ level with those of the observed suggests that the double minimum in the PES of the \tilde{B} state are slightly overestimated around the potential minimum since

the calculated value for the barrier to linearity is about twice the observed value. Nevertheless, we believe that the accuracy for the vibronic energies is adequate for calculating the FCFs and the transition probability for the $\tilde{X}-\tilde{A}$, $\tilde{X}-\tilde{B}$, and $\tilde{A}-\tilde{B}$ systems.

In the $\tilde{X} \rightarrow \tilde{A}$ excitation, the peak of Einstein's B coefficients among the same vibrational level for the \tilde{A} state shifted to lower levels of the \tilde{X} state than the corresponding FCFs. This originates in that the transition moment decreases with the increase of α and that the higher bending levels have larger α in average. In the same way, the peak of Einstein's B coefficients for the $\tilde{A} \rightarrow \tilde{B}$ excitation among the same vibrational level for the \tilde{B} state shifts to lower levels of the \tilde{A} state than the corresponding FCFs. On the other hand, the peak among the same vibrational level for the \tilde{A} state shifts to higher levels of the \tilde{B} state than the corresponding FCF. Fluorescence decay rates for the \tilde{A} and \tilde{B} states are evaluated from Einstein's B coefficients and the transition energies calculated in this study. The inverse of the sum of fluorescence decay rates for the pure bending levels of the \tilde{A} state agrees well with the observed lifetimes. This agreement would result in that the predicted lifetime for the \tilde{B} state is reliable. Current procedures are able to predict the vibrational transitions among the three electronic states of SiH₂ and SiD₂ with a sufficient accuracy.

ACKNOWLEDGMENT

The authors are very grateful to Dr. H. Ishikawa for providing the experimental data prior to publication and for useful discussion.

- ¹J. E. Rice and N. C. Handy, Chem. Phys. Lett. **107**, 365 (1984).
- ²Y. Yamaguchi, T. J. Van Huis, C. D. Sherrill, and H. F. Schaefer III, Theor. Chem. Acc. **97**, 341 (1997).
- ³Y. Muramoto, H. Ishikawa, and N. Mikami, J. Chem. Phys. (to be published).
- ⁴G. Duxbury, A. Alijah, and R. R. Tieling, J. Chem. Phys. **98**, 811 (1993).
- ⁵M. S. Gordon, Chem. Phys. Lett. **114**, 348 (1985).
- ⁶K. Balasubramanian and A. D. McLean, J. Chem. Phys. **85**, 5117 (1986).
- ⁷W. D. Allen and H. F. Schaefer III, Chem. Phys. **108**, 243 (1986), and references therein.
- ⁸S. Koseki and M. S. Gordon, J. Mol. Spectrosc. **123**, 392 (1987).
- ⁹W. Gabriel, P. Rosmus, K. Yamashita, K. Morokuma, and P. Palmieri, Chem. Phys. **174**, 45 (1993).
- ¹⁰I. Tokue, K. Yamasaki, and S. Nanbu, J. Chem. Phys. **119**, 5874 (2003).
- ¹¹D. E. Woon and T. H. Dunning, Jr., J. Chem. Phys. **98**, 1358 (1993), and references therein.
- ¹²M. R. A. Blomberg and P. E. M. Siegbahn, J. Chem. Phys. **78**, 5682 (1988).
- ¹³J. Simons, J. Phys. Chem. **93**, 626 (1989).
- ¹⁴S. R. Langhoff and D. E. Davidson, Int. J. Quantum Chem. **8**, 61 (1974).
- ¹⁵H.-J. Werner and P. J. Knowles, J. Chem. Phys. **89**, 5803 (1988).
- ¹⁶P. J. Knowles and H.-J. Werner, Chem. Phys. Lett. **145**, 514 (1988).
- ¹⁷MOLPRO is a package of *ab initio* programs written by H.-J. Werner, and P. J. Knowles with contributions from R. D. Amos, A. Berning, D. L. Cooper *et al.*,
- ¹⁸D. Shepard, Proceeding ACM National Conference 1968; P. Lancaster and K. Salkauskas, *Curve and Surface Fitting, An Introduction* (Academic, London, 1986), Chap. 10.
- ¹⁹K. C. Thompson, M. J. T. Jordan, and M. A. Collings, J. Chem. Phys. **108**, 8302 (1998), and references therein.
- ²⁰T. Ishida and G. C. Schatz, Chem. Phys. Lett. **314**, 369 (1999).
- ²¹J. V. Lill, G. A. Parker, and J. C. Light, Chem. Phys. Lett. **89**, 483 (1982).

- ²²D. T. Colbert and W. H. Miller, *J. Chem. Phys.* **96**, 1982 (1992).
- ²³E. M. Goldfield and S. K. Gray, *Comput. Phys. Commun.* **98**, 1 (1998).
- ²⁴C.-Y. Yang and S. K. Gray, *J. Chem. Phys.* **107**, 7773 (1997).
- ²⁵R. B. Lehoucq, K. Maschhoff, D. C. Sorensen, and C. Yang, ARPACK (Rice University, Houston, 1997); see the ARPACK homepage, <http://www.caam.rice.edu/software/ARPACK/>.
- ²⁶H. Eyring, J. Walter, and G. E. Kimball, *Quantum Chemistry* (Wiley, New York, 1944), p. 115.
- ²⁷C. Yamada, H. Kanamori, E. Hirota, N. Nishiwaki, N. Itabashi, K. Kato, and T. Goto, *J. Chem. Phys.* **91**, 4582 (1989).
- ²⁸R. Escibano and A. Campargue, *J. Chem. Phys.* **108**, 6249 (1998).
- ²⁹H. Ishikawa and O. Kajimoto, *J. Mol. Spectrosc.* **160**, 1 (1993).
- ³⁰J. Berkowitz, J. P. Greene, H. Cho, and B. Rušćić, *J. Chem. Phys.* **86**, 1235 (1987).
- ³¹S. P. Mort, N. A. Jennings, G. G. Balint-Kurti, and D. M. Hirst, *J. Chem. Phys.* **101**, 10576 (1994).
- ³²G. Herzberg, *Molecular Spectra and Molecular Structure, Infrared and Raman Spectra of Polyatomic Molecules* (Van Nostrand, Princeton, 1945), Vol. 2.
- ³³H. Ishikawa, Y. Muramoto, and N. Mikami, *J. Mol. Spectrosc.* **216**, 90 (2002).
- ³⁴E. Hirota and H. Ishikawa, *J. Chem. Phys.* **110**, 4254 (1999).
- ³⁵H. Ishikawa and O. Kajimoto, *J. Mol. Spectrosc.* **150**, 610 (1991).
- ³⁶L. Fredin, R. H. Hauge, Z. H. Kafafi, and J. L. Margrave, *J. Chem. Phys.* **82**, 3542 (1985).
- ³⁷M. Fukushima, S. Mayama, and K. Obi, *J. Chem. Phys.* **96**, 44 (1992).
- ³⁸J. S. Francisco, R. Barnes, and J. W. Thoman, Jr., *J. Chem. Phys.* **88**, 2334 (1992).
- ³⁹E. M. Goldfield, S. K. Gray, and L. B. Harding, *J. Chem. Phys.* **99**, 5812 (1993).
- ⁴⁰I. Dubois, *Can. J. Phys.* **46**, 2485 (1968).
- ⁴¹I. Dubois, G. Duxbury, and R. N. Dixon, *J. Chem. Soc., Faraday Trans. 2* **71**, 779 (1975).
- ⁴²See EPAPS Document No. E-JCPSA6-122-312515 for the Appendix. A direct link to this document may be found in the online article's HTML reference section. The document may also be reached via the EPAPS homepage (<http://www.aip.org/pubservs/epaps.html>) or from <ftp.aip.org> in the directory /epaps/. See the EPAPS homepage for more information.